Nonlinear Finite Element Modelling and Parametric Analysis of Shear Strengthening RC T-Beams with NSM CFRP Technique

Majid M. A. Kadhim, Ali Hadi Adheem & Akram R. Jawdhari

International Journal of Civil Engineering

ISSN 1735-0522

Int J Civ Eng
DOI 10.1007/s40999-018-0387-8

Springer

International Journal of Civil Engineering
https://doi.org/10.1007/s40999-018-0387-8

RESEARCH PAPER

Nonlinear Finite Element Modelling and Parametric Analysis of Shear Strengthening RC T-Beams with NSM CFRP Technique

Majid M. A. Kadhim[1,2] · **Ali Hadi Adheem**[3] · **Akram R. Jawdhari**[1,4]

Received: 25 July 2018 / Revised: 26 November 2018 / Accepted: 10 December 2018

Abstract
In this study, a robust three-dimensional finite element (FE) model has been developed for reinforced concrete beams strengthened in shear with near surface mounted (NSM) carbon fibre reinforced polymer (CFRP) rods. The FE models were developed and validated against existing experiments and presented various nonlinear constitutive material laws and interfacial relations. A detailed parametric study was performed to investigate the effects of various parameters on the performance of strengthened member. It was shown that increasing the concrete compressive strength (f_c') from 20 to 50 MPa, leads to an increase in the beam's ultimate load and contribution of NSM CFRP reinforcement. While for NSM reinforcement ratio (ρ_f), the ultimate load slightly increased when ρ_f is 0.14–0.22%, and then increased by 11% in average when ρ_f increased to 0.28%. Varying the percentage of existing steel stirrups (ρ_{sw}) from 0.11 to 0.36%, leads to an increase in ultimate load from 8 to 15% compared to the control un-strengthened specimen. However, the further increase in ρ_{sw} (more than 0.36%) caused a reduction in the contribution of NSM CFRP technique because of the changing in the failure mode. The distance between existing steel stirrups and NSM reinforcement does not affect the behaviour. In addition, the model predictions were used to evaluate several design formulas available in the literature for this technique. It was found that some theoretical equations were conservative as long as the governing failure mode is shear.

Keywords NSM FRP technique · Shear · Finite element method · RC beam · Debonding · Bond-slip law

1 Introduction

The use of fibre reinforced polymer (FRP) material in the construction industry has seen a steady growth over the last few decades, in various applications such as in construction of new structures or repair/upgrade of old ones. Due to their excellent attributes such as high tensile strength, corrosion resistance, good fatigue performance, and ease of handling and installation [1, 2], FRP composites have been used extensively and successfully in strengthening and repairing members deficient in axial, shear, bending, or torsion [3–6]. Externally bonded FRP (EB FRP) reinforcement such as sheets or plates is used widely to retrofit concrete, steel and masonry structures. One of the prominent uses of EB FRP reinforcement is the shear strengthening of reinforced concrete (RC) beams/girders, which typically require strengthening due to insufficient shear strength or due to flexural upgrade [7].

EB FRP shear reinforcement can be applied to cover only the beam sides (side bonding); sides and bottom (U-jacketing); or all four faces (complete wrapping) [8]. Over the last two decades, shear retrofit with EB FRP has established a strong popularity due to extensive experimental works, numerical and analytical studies, field applications, and attention in code provisions [7–13]. Experimental tests have reported a significant increase of shear capacity for concrete beams strengthened with EB FRP ranging from

✉ Majid M. A. Kadhim
majid.kadhim@manchester.ac.uk;
eng.majid.mohammed@uobabylon.edu.iq

Ali Hadi Adheem
ali.hadi@kit.edu.iq

Akram R. Jawdhari
akram.hassan@uky.edu

[1] College of Engineering, University of Babylon, Hilla, Iraq

[2] School of Mechanical, Aerospace and Civil Engineering, University of Manchester, Manchester, UK

[3] Kerbala Technical Institute, Al-Furat Al-Awsat Technical University, Kerbala 56001, Iraq

[4] Department of Civil Engineering, University of Kentucky, Lexington, USA

Published online: 01 March 2019

29 to 135% [1–12], in comparison with un-strengthened specimens. Governing parameters were also examined extensively, including number of strips, inclination angle, spacing between strips, adhesive type, and anchorage [7].

Another use of FRP reinforcement is in the near surface mounted (NSM) strengthening system, referred to for brevity as NSM FRP, which gained a wide attraction and proved to be a viable option for retrofit of concrete structures [3, 14, 15]. When compared to EB FRP, NSM FRP technique has a number of advantages including lower demands for surface preparation and better protection against environmental exposure and damage by fire, impact, vandalism [7, 15]. In flexural retrofits of negative moment regions, NSM is favoured over EB, which is typically subject to mechanical and environmental damage [15]. While in shear retrofits, NSM is less prone to debonding failure, and can easily be prestressed and/or anchored to the member [3, 7].

Until the mid-2000s, shear retrofit by NSM FRP system was still an emerging technique [7]. However, within the few last years, there has been a surge in research activities, in an apparent effort to establish a sound foundation for the method in both shear and flexural retrofits [3, 14–17]. Existing experimental results assertively confirmed the effectiveness of this technique in enhancing the shear capacity of RC beams. For instance, Al-Mahmoud et al. [3] tested seven RC beams, which had dimensions of 2000 × 150 × 200 mm (length × width × height) and were strengthened in shear with 6 mm sand-coated NSM CFRP rods, under four-point and three-point bending schemes. The increase in shear strength, compared to beams having conventional steel stirrups, was 43.6% for beams with epoxy resin, and 34.6% for beams with cementitious mortar. The effects of factors governing the behaviour of NSM CFRP shear strengthening, including percentage and inclination of NSM reinforcement, percentage of the existing steel stirrups and concrete compressive strength, were investigated experimentally through a series of tests [18–24].

Despite the large number of experimental and analytical studies on the shear strengthening of RC beams with CFRP NSM rods, number of FE studies is still very limited. A detailed search on the literature revealed only few FE studies on RC beams strengthened in shear with NSM FRP rods [25–28]. For example, the numerical study by Sabol and Priganc [25] included three FE models for simply supported rectangular RC beams tested in four-point bending. Sakar et al. [26] simulated the performance of cantilever RC beams under cyclic loading at the free end of the beam, by three-dimensional (3D) FE models. The need for FE analyses stems from the unrivalled capabilities of FE models in providing an in-depth and unlimited examination of different outputs (forces, stresses, strains, etc.) of the strengthened member, strengthening reinforcement, and the interface between them. In addition, due to their low cost when compared with laboratory tests, FE models can be utilized to perform parametric studies to evaluate the effects of different variables and to optimize the design of the member or system.

The present study is aimed at expanding the available database on FE simulations of NSM CFRP shear strengthening and presenting FE models capable of accurately predicting the behaviour of strengthened RC members. Although the FE models were developed and validated for the experimental work conducted by De Lorenzis and Nanni [17], they intend to provide a comprehensive understating of the effects of larger number of variables that may affect the contribution of this technique. By understanding the effects of these parameters on the response of strengthened member, ultimately a precise design guide can be established, thus allowing practitioners to benefit from the considerable advantages of this technique. The parameters evaluated were: concrete compressive strength in conjunction with various CFRP percentages, relative distance between existing steel stirrups and CFRP rods, and percentage of existing steel stirrups. In addition, the accuracy of several available analytical formulas used to predict the shear capacity of NSM strengthened RC members is validated by comparing their predictions with those obtained from the FE simulations.

2 Experimental Program

The experimental study consisted of five, full-scale RC T-beams tested under four-point bending [17]. The test matrix comprised two un-strengthened beams, one without internal steel stirrups and one with internal steel stirrups, and three beams strengthened in shear with no. 3 ($\phi = 9.5$ mm) NSM CFRP rods varying by rod spacing (either 127 or 178 mm) and anchorage by embedment into the beam flange, Table 1. Flexural reinforcement (Fig. 1) consisted of two no. 9 ($\phi = 28.65$ mm) for tension and two no. 4 ($\phi = 12.7$ mm) for compression, only in specimens with internal steel stirrups.

The reported compressive strength of concrete was 31 MPa. The yield strength of flexural and shear steel reinforcements was 427 and 346 MPa, respectively. Material properties of the CFRP rod were 1875 MPa and 104.8 GPa, for the tensile strength and elastic modulus, respectively. Tensile and compressive strengths of adhesive material, which was used as a filling material for CFRP rods, were 13.8 and 55.2 MPa, respectively. In the tests, one-half of each beam was intentionally over reinforced in shear to ensure controlled shear failure in the other half and to facilitate monitoring and instrumentation [17].

Obtained results were very encouraging, were the use of NSM FRP rods resulted in an increase of the beam's shear capacity of 35% for the specimen with internal shear stirrups, and 106% for the specimen without shear stirrups. The

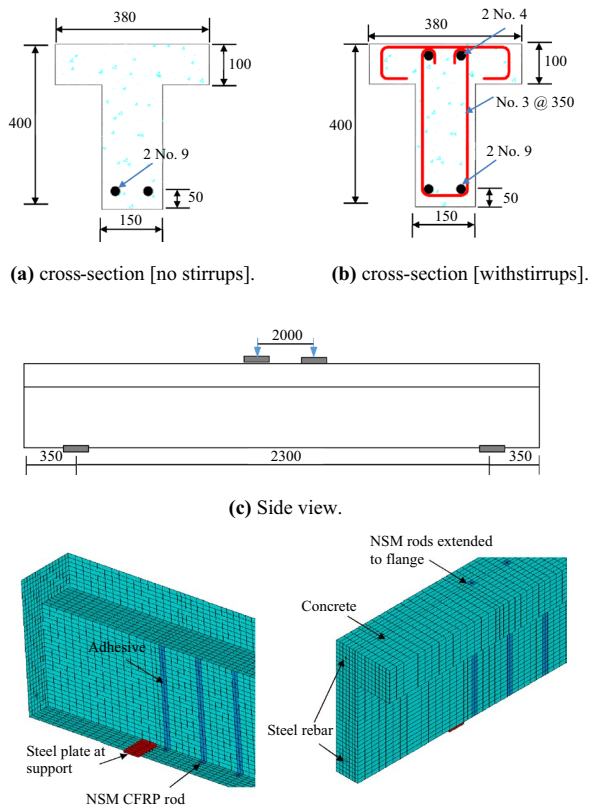

(a) cross-section [no stirrups]. **(b)** cross-section [withstirrups].

(c) Side view.

(d) FE model, showing different components.

Fig. 1 Full-scale T-beams tested by De Lorenzis and Nanni [29], dimensions in mm

failure mode was either (a) debonding of one or more rods in conjunction with splitting of epoxy layer, or (b) separation of concrete cover at the longitudinal steel reinforcement.

3 Finite Element Modelling

The three-dimensional model is built using the general purpose FE ANSYS software [29]. To reduce computational efforts, desk space, and running time, a full-length/half-width model was used (Fig. 1d) utilizing available symmetry conditions, which were only in cross-section. The difference between shear reinforcement in control and test sides prevented symmetry in the length direction, and required using full-length model. To accurately predict the peak load and post-peak response, load was applied in a displacement control approach via induced deflection at the loading points, instead of a force-control loading. The following sections describe various components of the FE model. Full Newton–Raphson integration method is used to solve the highly nonlinear structure, using multiple load steps and a convergence criterion of 4% and 8% for displacements and loads, respectively.

3.1 Elements Description

The concrete volume was meshed using the conventional concrete element (SOLID65), which has eight nodes and three translational degrees of freedom (DOF) per node, with capabilities including crushing in compression, cracking in tension, nonlinear stress–strain behaviour, creep, etc. The flexural and shear steel reinforcement and CFRP rods were meshed using the truss element (LINK18), which has two nodes and three translational DOF per node and can incorporate steel plasticity and FRP material failure.

The adhesive of NSM rods was modelled by the brick element (SOLID185), which also has eight nodes and three translational degrees of freedom (DOF) per node. This element was also used to model steel plates that were utilized in the experiment at loading and support locations. The last part of the model is the interaction between the adhesive and concrete which was modelled using surface-to-surface contact elements. Following ANSYS recommendations, concrete was selected to be the target surface, modelled with TARGE170 element, and adhesive chosen to be the contact surface, modelled using CONTA173 element. The contact element is defined by four nodes, with three translational nodal DOFs. Further details concerning the modelling of adhesive–concrete interface are given in Sect. 3.3.

3.2 Material Modelling

3.2.1 Concrete

A nonlinear uniaxial stress–strain model for concrete, developed by Kent and Park [30], was used to simulate the concrete compressive behaviour up to the maximum strength (f_c') (Fig. 2a). The model can be presented mathematically by the following equation:

$$f_c = f_c' \left[2\left(\frac{\varepsilon}{\varepsilon_0}\right) - \left(\frac{\varepsilon}{\varepsilon_0}\right)^2 \right], \tag{1}$$

where f_c is the concrete compressive stress at any strain (ε); ε_0 is the strain at maximum compressive strength f_c', which can be calculated from the following equation:

$$\varepsilon_0 = \frac{2f_c'}{E_c}, \tag{2}$$

where E_c is the elastic modulus of concrete, determined from ACI code (ACI 318 [31]) as following:

$$E_c = 4700\sqrt{f_c'}. \tag{3}$$

After the compressive stress in concrete reaches f_c', the concrete behaviour is assumed to be partially confined

because of the lateral support from steel stirrups and/or NSM CFRP shear reinforcement. Chansawat et al. [32] suggested a linear descending model for the post-peak stress–strain curve of RC beams confined by FRP sheets, which is adopted herein for the beams strengthened in shear by steel stirrups and/or NSM CFRP bars. The descending portion terminates at a stress of $0.3f_c'$, and its slope (E_{c2}) (Fig. 2a) can be determined from the following equation:

$$E_{c2} = 0.018E_c. \tag{4}$$

The concrete tensile stress–strain behaviour is modelled as a linear elastic prior to the start of cracking at a maximum tensile stress which can be obtained from ACI code [31] using the following equation:

$$f_t = 0.56\sqrt{f_c'}. \tag{5}$$

Tension-stiffening effects are modelled with a linear descending curve ending at a strain of $6\varepsilon_t$, where ε_t is the strain at f_t (Fig. 2b). The model was defined in ANSYS by providing the values for f_t, E_c, and stress relaxation factor ($0.6f_t$, Fig. 2b). Ultimate strain ($6\varepsilon_t$) and shape of the curve (i.e. linear) are software pre-set inputs which cannot be altered. A value of 0.3 was used for the open and closed shear transfer coefficients [33, 34]. The Poison's ratio (ν) of concrete is assumed to be 0.2 [33, 34].

3.2.2 NSM CFRP Reinforcement

A linear elastic model is employed for the CFRP reinforcement (Fig. 2c). The main input values for this model

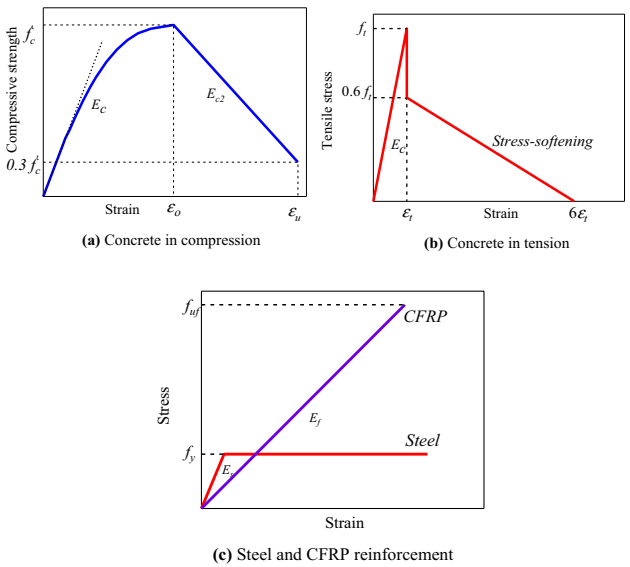

(a) Concrete in compression

(b) Concrete in tension

(c) Steel and CFRP reinforcement

Fig. 2 Constitutive material models

were listed in Sect. 2. A value of 0.35 was assumed for ν, following recommendation of Omran and El-Hacha [35].

3.2.3 Steel Reinforcement

In the FE models, the steel reinforcement was modelled as an elastic–perfectly plastic material (Fig. 2c). The elastic modulus (E_s) and Poisson's ratio (ν) were 200 GPa and 0.3, respectively [4]. Other material properties including yield and ultimate strength of steel are listed in Sect. 2. Linear elastic model was assumed for the steel plates at support and loading, with E_s and ν, identical to the above values.

3.3 Interface Modelling

The word "interface" here refers to the concrete–adhesive interface which is the weakest joint in the NSM technique. This interface was modelled using contact-target element pairs and cohesive zone material (CZM) model, applicable for tangential (shear) debonding, normal (peeling) debonding, and mixed-mode debonding. For the RC beams strengthened in shear with NSM CFRP rods, a mixed-mode debonding model was adopted to produce more realistic predictions if shear and peeling forces are both present at the interface [35].

To define the interface as a mixed-mode CZM, the following input values should be introduced including the maximum normal contact stress, normal fracture energy, maximum contact shear stress and shear fracture energy. Bilinear bond-slip curves available in ANSYS were used to represent the individual normal and shear interfacial behaviours, Fig. 3. It can be seen from this figure that debonding initiates when $d_m = 0$ and is completed when $d_m = 1$. The values of shear and normal contact stresses can be calculated as follows:

$$\tau_t = K_t\delta_t(1 - d_m), \tag{6}$$

$$\sigma_n = K_n\delta_n(1 - d_m), \tag{7}$$

where τ_t and σ_n are the shear and normal contact stresses, respectively, K_t and K_n are the shear and normal contact stiffnesses, respectively, δ_t and δ_n are the relative movement in the tangential and normal directions (slip and gap), respectively, and d_m is the debonding parameter which can be obtained from the following equation:

$$d_m = \left(\frac{\Delta_m - 1}{\Delta_m}\right)\chi, \tag{8}$$

in which Δ_m and χ are defined as:

$$\Delta_m = \sqrt{\left(\frac{\delta_n}{\bar{\delta}_n}\right) + \left(\frac{\delta_t}{\bar{\delta}_t}\right)}, \tag{9}$$

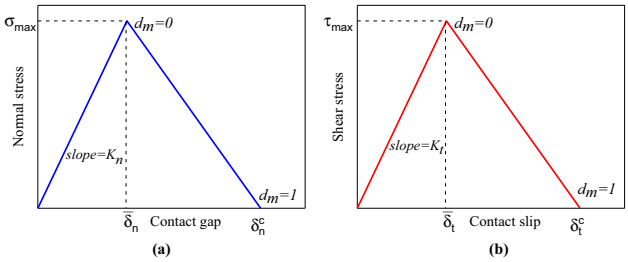

Fig. 3 **a** Bilinear normal stress-gap and **b** bilinear shear stress–slip models

$$\chi = \frac{\delta_n^c}{\delta_n^c - \bar{\delta}_n} = \frac{\delta_t^c}{\delta_t^c - \bar{\delta}_t}, \tag{10}$$

where $\bar{\delta}_n$ and $\bar{\delta}_t$ are the contact gap at the maximum normal stress and the slip at the maximum shear stress, respectively, δ_n^c and δ_t^c are the contact gap and slip at the completion of debonding (see Fig. 3), respectively.

Numerical values needed to define the first part of the mixed-mode model, i.e. the shear stress–slip relation, were obtained from the theoretical bond-slip relation proposed by Seracino et al. [36] and reproduced as follows:

$$\tau_{max} = (0.802 + 0.078\varphi){f_c'}^{0.6}, \tag{11}$$

$$G_{ct} = \frac{0.976\varphi^{0.526}{f_c'}^{0.6}}{2}, \tag{12}$$

where τ_{max} is the maximum contact shear stress, φ is the aspect ratio of the interface failure plane which can be calculated as in Eq. 13, f_c' is the compressive strength of concrete and G_{ct} is the shear fracture energy,

$$\varphi = \frac{\text{Groove depth} + 1\ \text{mm}}{\text{Groove width} + 2\ \text{mm}}. \tag{13}$$

On the other hand, the normal stress-gap model is developed by assuming that debonding in normal direction occurs when the normal stress exceeds the concrete tensile strength which was defined earlier in Eq. 5 [36, 37]. The normal fracture energy is also assumed to be equal to the concrete fracture energy suggested by CEB-FIB code [38] (see Eq. 15),

$$G_{cn} = G_{fo}\left(\frac{f_c'}{10}\right)^{0.7}, \tag{14}$$

where σ_{max} is the maximum normal contact stress, G_{cn} is the normal fracture energy and G_{fo} is the base value of fracture energy depending on the maximum aggregate size. The fracture energies, G_{ct} and G_{cn}, represent the areas under the stress–slip/gap models and can be used to determine δ_c^t and δ_c^n as follows:

$$G_{ct} = 0.5\tau_{max}\delta_c^t, \tag{15}$$

$$G_{cn} = 0.5\sigma_{max}\delta_c^n. \tag{16}$$

The CZM model was assigned to the contact-target elements via an ANSYS command subroutine. Table 2 lists the numerical values used to define the CZM model, based on Eqs. 11–14. It should be noted that values in Table 2 are only applicable for the validation models of De Lorenzis and Nanni [17] specimens; while for the FE models in parametric analysis, new values are calculated based on the utilized material and geometric properties. To overcome convergence difficulties as a result of debonding during material softening, ANSYS introduces an artificial damping coefficient, which is given a value based on the smallest element size [29].

4 Validation of the FE Model

To validate and calibrate the FE model, numerical predictions were compared to the test results in De Lorenzis and Nanni [17] tests in terms of load–deflection curve, ultimate load, failure mode and strain profile. The authors conducted a mesh sensitivity analysis to ensure obtaining accurate results from the FE models, while using the minimum number of elements and nodes. It was found that

Table 1 Beam test matrix, from [29]

Beam code	Steel stirrups		NSM CFRP rods		
	Quantity	Spacing (mm)	Quantity	Spacing (mm)	Anchorage in flange
BV	–	–	–	–	–
B90-7	–	–	2φ9.5 mm	178	No
B90-5	–	–	2φ9.5 mm	127	No
B90-5A	–	–	2φ9.5 mm	127	Yes
BSV	2φ9.5 mm	356	–	–	–

a 5-mm mesh size provided divergence of less than 1% compared to the finer mesh sizes.

Figure 4 shows the load against mid-span deflection comparisons between tests and FE models, for specimens BV, B90-7, B90-5, and B90-5A. This comparison demonstrates that the FE model was able to capture the load–deflection curve with an accepted level of accuracy. In addition, Table 3 lists the numerically obtained and experimentally recorded ultimate loads, the difference between these loads, and the failure mode from experiment or model. The table shows that the predicted ultimate load was in good agreement compared to experimental results with a maximum divergence of 7%.

Regarding the failure modes, it can be seen in Table 3 that the model was able to capture the failure modes reported experimentally. For example, beam B90-7 failed by debonding of one or more CFRP rods which is identical to what took place in the FE model as shown in Fig. 5a. This figure shows that the shear cracks obtained from FE simulation of beam B90-7 was almost similar to those measured in the experiment. In addition, the FE model was able to capture the debonding failure that occurred in this beam for some CFRP rods as shown in Fig. 6. It can be noticed from this figure that the contact status for the CFRP rod (located 356 mm away from the beam mid-span) was sticking/no debonding (status no. 3, Fig. 6) from the start of loading until a load (P) of 310 kN. When P is increased further, contact status changed to sliding (status no. 2, Fig. 6) to indicate initiation of debonding process. This stage continued until ultimate load is reached, and debonding is completed, which is represented by contact status no. 1 in Fig. 6.

Furthermore, Fig. 5b illustrates the crack pattern of beam BSV obtained from the numerical and experimental results. It can be seen from this figure that the numerical model was able to predict the crack pattern occurred in the experiments with high level of accuracy.

5 Design Approach

A verified design model is required in order for the shear strengthening by NSM CFRP technique to become accepted as a reliable method that can be used in everyday engineering practices. Hence, this section highlights the available design rules and compares their results with the experimental and numerical data obtained in the current paper to find their applicability with a wide range of database.

Generally, the nominal shear strength of RC beams strengthened with externally bonded CFRP can be calculated by adding a third term to the basic equation [17] provided by ACI code [31], as in Eq. 17:

$$V_u = \phi\left[\left(V_c + V_s\right) + \psi V_f\right], \tag{17}$$

where ϕ is the strength reduction factor for shear strengthening of RC elements which has a value of 0.85 as indicated by ACI [31]. ψ is an additional reduction factor for the case of externally bonded CFRP, with an assumed value of 0.85 as recommended by ACI 440 committee [13]. The values of V_c and V_s are the contributions of concrete and steel stirrups, respectively—which may be computed according to standard concrete design codes. V_f represents the contribution of NSM CFRP reinforcement to shear.

Since the study is aimed at investigating the contribution of NSM CFRP strengthening technique, the focus of this section is on the expressions used to predict the contribution from the composite, while calculations concerning the contribution of concrete and conventional steel reinforcement can be found elsewhere in the literature. Two analytical formulations that are widely used to predict the contribution of NSM reinforcement will be presented in this section to compare their predictions with the numerical and experimental results.

5.1 Formulation by Nanni et al. [16]

Based on the formulation proposed by Nanni et al. [16], the value of V_f can be found as in following:

$$V_f = 2\pi\, d_b\, \tau_b L_{tot\,min} \sin\theta_f, \tag{18}$$

where d_b is the diameter of CFRP bar, τ_b represents the average bond stress of the CFRP rods—which is equal to 6.9 MPa as recommended by De Lorenzis and Nanni [17] based on results obtained from bond tests, $L_{tot\,min}$ is the minimum value of the sum of effective bond lengths of each bar crossed by a crack, and θ_f is the angle of CFRP bar relative to the beam longitudinal axis.

5.2 Formulation by Dias and Barros [18]

The contribution of CFRP bars can be obtained as in Eq. 19, following the formulation suggested by Dias and Barros [18].

$$V_f = h_w \frac{A_{fv}}{s_f} \varepsilon_{fe} E_f \left(\cot\alpha + \cot\theta_f\right) \sin\theta_f, \tag{19}$$

Table 2 Input values for the contact elements

Property	Value
τ_{max} = Maximum contact shear stress	6.881 MPa
G_{ct} = Shear fracture energy	3.735 N/mm
σ_{max} = Maximum normal contact stress	3.342 MPa
G_{cn} = Normal fracture energy	0.077 N/mm
η = Artificial damping coefficient	0.001

where h_w is the web depth of the beam, A_{fv} is the area of two CFRP bars, s_f is the spacing of the bars, ϵ_{fe} represents the effective strain, E_f is the elastic modulus of the CFRP and α represents the orientation of the shear failure crack.

6 Parametric Study

6.1 Concrete Compressive Strength

One of the most important parameters affecting the contribution of NSM shear reinforcement is the compressive strength of concrete (f_c'). Previous studies [20, 22, 24] revealed that the higher f_c' is, the higher NSM CFRP effectiveness gets. However, this conclusion was drawn by investigating a limited range of f_c' with limited CFRP percentages (ρ_f)—which can be calculated from Eq. 20. Thus, in the present study, a wide range of f_c', 20–50 MPa, will be investigated for various CFRP percentages. In this section, beam B90-7 is used to study the effects of this parameter. For each value of f_c', three CFRP percentages are adopted, $\rho_f = 0.28\%$, 0.22% and 0.14%, corresponding to CFRP rod diameters of 12, 9.5 and 6 mm, respectively. The spacing between rods was kept constant and equal to 178 mm.

$$\rho_f = \frac{2\pi d_b}{b_w s_f} \times 100. \tag{20}$$

It can be seen from Fig. 7 that increasing f_c' leads to increasing the ultimate load (or effectiveness of NSM reinforcement). This stems from the coupling effects concrete strength has on the total shear strength of NSM-strengthened RC beam, by increasing the concrete shear contribution in Eq. 17, and also by delaying the debonding failure of NSM reinforcement. The shear and normal bond strengths of the NSM–concrete interface and their corresponding fracture energies are all dependent on f_c', as can be observed from Eqs. 11 to 14. Considering the effects of ρ_f, the ultimate load slightly increases when ρ_f is 0.14–0.22%. A sharp increase in ultimate load, in an average of 11%, is seen when ρ_f is 0.28%.

The comparison between the simulation results and predictions of the design approaches described in Sect. 5 showed that the predictions of these equations are always less than the corresponding FE values as shown in Fig. 8. In other words, if the ratio between the ultimate load obtained from the FE simulations and analytical predictions considered as a factor the so-called k ($k = V_u^{FE}/V_u^{ana}$), the value of this factor is more than 1.0 for all studied cases.

Particularly, when the formulation proposed by Nanni et al. [16] is used, the average values of k are 1.16, 1.10 and 1.16 for the CFRP percentages 0.14%, 0.22% and 0.28%, respectively, while for the Dias and Barros [18] formulation the average k values are 1.49, 1.32 and 1.35 for the same respective CFRP percentages. It can also be seen from Fig. 8 that ultimate load values predicted by both design rules are quiet conservative regardless of the compressive strength and the CFRP percentage. It can be concluded from the above discussion that the proposed design approaches can conservatively predict the ultimate load of RC beams strengthened in shear with NSM CFRP rods.

Table 3 Comparison between FE and experimental results

Specimens	Ultimate load (kN)			Failure mode	
	Experimental	FE	Difference %	Experimental	FE
BV	180.6	176.4	2.3	SC	SC
B90-7	230.4	236.8	−2.8	BF	BF
B90-5	255.3	236.7	7.3	BF	BF
B90-5A	371.4	347.9	6.3	SP	SP
BSV	307.0	308.2	−0.4	SC	SC

SC shear compression, *BF* bond failure, *SP* splitting of concrete cover

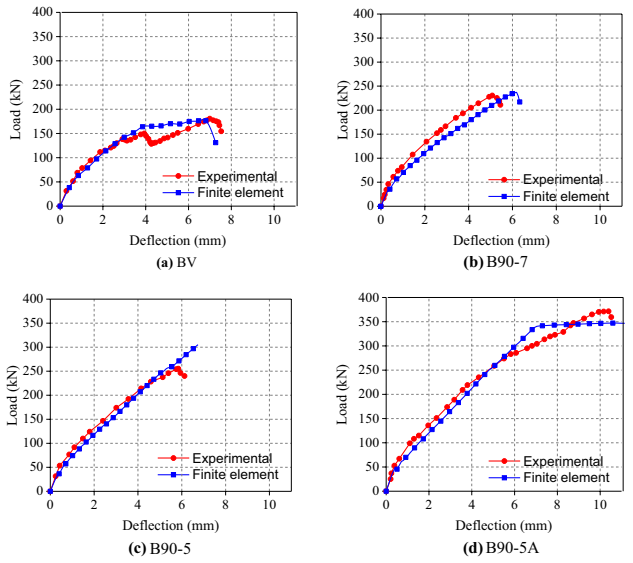

Fig. 4 Comparison of load–deflection curves from FE model and experimental tests

6.2 Percentage of Existing Shear Reinforcement

Typically, NSM technique is used to strengthen/repair existing members which are expected to have various ratios of existing shear reinforcements, in the form of steel stirrups. Consequently, it is important to investigate whether the NSM retrofit is equally effective for all different existing shear reinforcement ratios (ρ_{sw}) or not. The influence of ρ_{sw} was studied by [18, 39]. Dias and Barros [18] found that the contribution of NSM CFRP technique in shear was reduced when the percentage of internal steel stirrups (ρ_{sw})

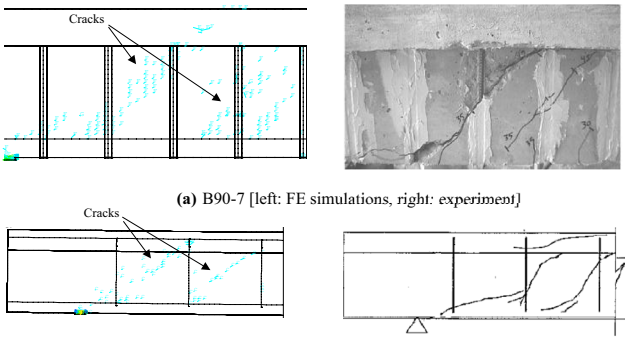

(a) B90-7 [left: FE simulations, right: experiment]

(b) BSV [left: FE simulations, right: experiment]

Fig. 5 Comparison of failure modes obtained from experimental and FE simulations, **a** specimen B90-7; **b** specimen BSV

was increased. This observation was obtained by testing a series of RC beams with ρ_{sw} ranging from 0.1 to 0.17%. However, Mofidi et al. [39] analysed a database of more than

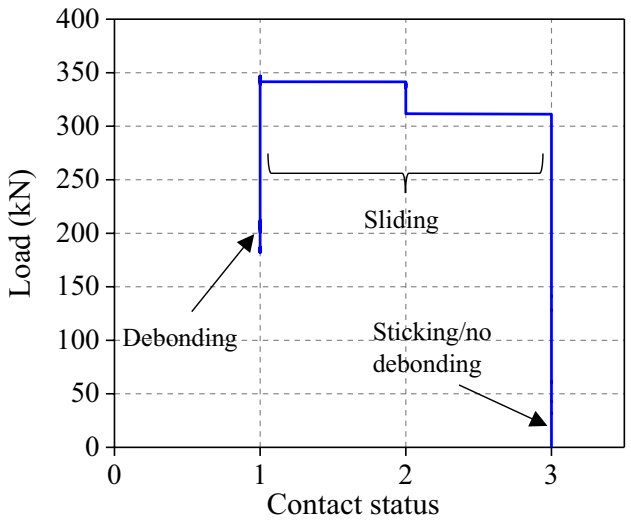

Fig. 6 Contact status against the applied load for beam B90-7

69 RC beams strengthened with NSM CFRP and found that increasing ρ_{sw} led to an increase in the effectiveness of CFRP reinforcement, which contradicts Dias and Barros [18] findings. Accordingly, further research and discussion is needed to clarify this parameter and its effects.

In this study, the effects of ρ_{sw} were examined numerically by adopting a wide range of the percentage of existing steel reinforcement (ρ_{sw}). In each percentage, one un-strengthened beam and one strengthened beam with NSM CFRP rods, having a diameter of 9.5 mm and a spacing of 178 were analysed. All other material and geometrical inputs were similar to beam B90-7, as discussed in Sect. 3. The following equation is used to define ρ_{sw} when developing the numerical model:

$$\rho_{sw} = \frac{A_{sw}}{b_w \times S_w} \times 100, \tag{21}$$

where A_{sw} is the cross-section of the arms of a steel stirrups, b_w is the width of beam's web and S_w is the spacing of the stirrups.

The simulation results demonstrated that the contribution of NSM CFRP technique was affected by ρ_{sw} as shown in Fig. 9. It can be seen from this figure that the contribution of NSM technique (the vertical axis in Fig. 9 which represents the difference between the ultimate load of strengthened and un-strengthened beams for a specific ρ_{sw} divided by the ultimate load of the un-strengthened beam) increased from 8 to 15% when ρ_{sw} was varied from 0.11 to 0.36%.

However, further increase in ρ_{sw} value caused a reduction in the contribution of NSM reinforcement. The reason for this reversal in behaviour is the change in failure mode. When ρ_{sw} was $\leq$0.36%, the failure mode was debonding in one or more CFRP bars due to splitting of the adhesive cover in the grooves followed by global shear failure, as shown in Fig. 10a. While for $\rho_{sw} >$ 0.36%, the failure mode was flexure, as shown in Fig. 10b.

Figure 10a shows the slip distribution at the contact surface between adhesive and concrete cover for several CFRP rods, at ultimate stage. It can be noticed from this figure that the maximum slip from the model predictions was 1.07 mm. This value is larger than the theoretical slip of 0.27 mm (determined from Eq. 15 and shown in Table 2) at completion of debonding, indicating that splitting of adhesive from the concrete cover has already occurred for several rods (Fig. 10).

Based on the above results, the contribution of NSM strengthening technique can be estimated from the percentage of existing steel reinforcement as in Eq. 22, which was obtained from simple statistical analysis of Fig. 9. It should be noticed that Eq. 22 was derived from the results of this section in which the percentage of CFRP reinforcement, concrete compressive strength and beam dimensions were constant. Further research is required to generalize this equation and apply its predictions for other cases. When verified, Eq. 22 can be added to the previously suggested equations (in Sect. 5) to include the combined effects of steel stirrups and NSM CFRP reinforcement.

$$\begin{aligned} V_f\% &= 0.266{\rho_{sw}}^{0.592} \times 100\% \quad \rho_{sw} \leqslant 0.36, \\ V_f\% &= 0.061{\rho_{sw}}^{-1.166} \times 100\% \quad \rho_{sw} > 0.36. \end{aligned} \tag{22}$$

Regarding evaluating the predictions of design formulas in Sect. 5, these approaches seem to be conservative for most ρ_{sw} (Fig. 11). However, when ρ_{sw} was greater than 0.36%, the predicted ultimate load from the formulation by Nanni et al. [16] was unsafe compared to FE results. This occurred because the failure mode of the beams with $\rho_{sw} \geqslant 0.36\%$ was flexural. Generally, Dias and Barros [18] formulation provides over-conservative predictions for ultimate loads compared to the corresponding FE values, with an average value of 1.6 for k. As a future recommendation, more studies are required to investigate the combined effects of existing shear reinforcement and additional NSM reinforcement.

6.3 Distance Between Existing Shear Reinforcement and NSM Rods

The relative position between internal steel stirrups and applied CFRP reinforcement, hereafter referred to as $x_{nsm\text{-}st}$, may have a significant contribution to the effectiveness of CFRP shear configuration. It was found that when the applied NSM reinforcement intercepts the existing steel stirrups, it causes a debonding of the NSM bars/strips [24]. However, this observation was found by testing only two beams with a small clearance of 7 mm between steel stirrups and NSM rods, which might have promoted spalling of the concrete cover and debonding failure. On the other hand and for the current experimental work [17], the rod/stirrup clearance is large, at 40 mm and concrete spalling and early debonding are not expected.

To investigate this parameter, BSV beam is strengthened with three different CFRP configurations as shown in Fig. 12, corresponding to $x_{nsm\text{-}st}$ of 0, 45, and 89 mm. The distance between the CFRP rods is the same (178 mm) as in beam B90-7. The simulation results showed that the difference in ultimate load for the beams strengthened in various CFRP configurations is negligible when the maximum difference was less than 0.2%. This finding is not in agreement with those obtained by Dias and Barros [24]. The main reason for this (as reported in this section) is related to the fact that the remaining concrete cover after cutting the grooves was 7 mm in the experimental work performed by Dias and Barros [24], while for the current simulation is 21 mm.

In addition, strain profiles in the longitudinal direction along the CFRP rod located 534 mm away from the beam centerline are plotted in Fig. 13 for various CFRP configurations. This figure demonstrates that the effect of CFRP configuration is trivial when the maximum difference along the strain profile was less than 6% for all CFRP configurations. This comparison reflects the minor influence of the relative distance between the steel stirrups and applied CFRP rods.

As a design note and given the miniature effects of $x_{nsm\text{-}st}$, it is not recommended to apply NSM reinforcement directly on top of existing steel stirrups as this might cause disruption in the concrete between the two reinforcements and promotes premature debonding in NSM, particularly if the remaining concrete cover between the rods and stirrups is small.

7 Conclusions

This paper investigated the effectiveness of NSM CFRP rods as a shear strengthening system for RC beams, employing robust three-dimensional finite element models. The following conclusions could be drawn from the results obtained:

1. The numerical model presented was capable of capturing the response of the RC beams strengthened in shear with NSM CFRP rods, in terms of load-deflection history, ultimate load, and failure modes.
2. Increasing the concrete compressive strength (f_c') from 20 to 50 MPa led to an increase in ultimate load of strengthened beam. f_c' contributes twofold, by increasing the shear component by concrete and by delaying debonding failure of NSM reinforcement.
3. Considering the effects of NSM reinforcement ratio (ρ_f), the ultimate load slightly increases when ρ_f is 0.14–0.22%. A sharp increase in ultimate load, in average of 11%, is seen when ρ_f is 0.28%.
4. The effectiveness of NSM strengthening technique in shear is governed by the percentage of existing steel stirrups (ρ_{sw}). When ρ_{sw} is increased from 0.11 to 0.36%, the ultimate load increased from 8 to 15%, compared to the un-strengthened samples. However, when further increase was applied for ρ_{sw} the contribution of NSM strengthening technique reduced to be 8%.
5. The simulation results also revealed that the contribution of the NSM technique is not dependent on the relative distance between the existing steel stirrups and the added CFRP bars. However, it is not recommended to

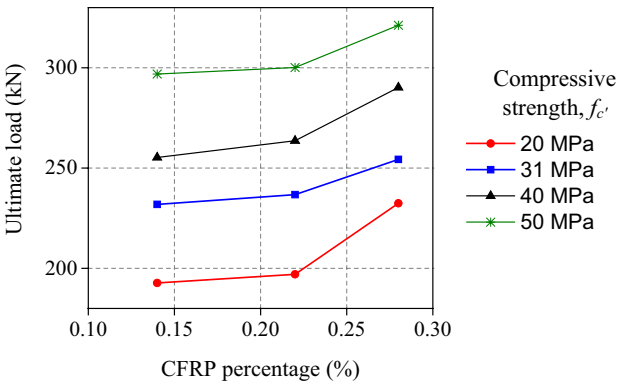

Fig. 7 Effect of concrete compressive strength on the effectiveness of NSM technique with varying CFRP percentages

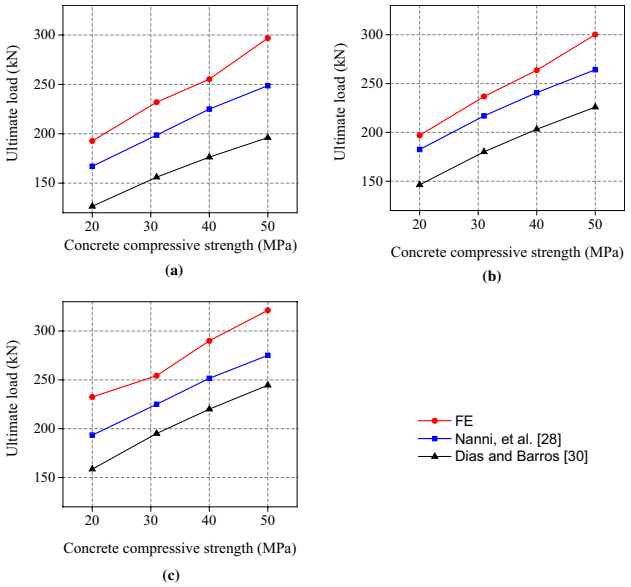

Fig. 8 Comparison between the FE results and predictions of design approaches for different CFRP percentages **a** 0.14%; **b** 0.22%; **c** 0.28%

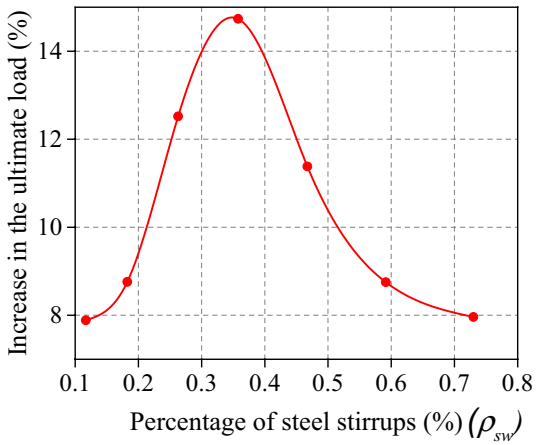

Fig. 9 Contribution of NSM CFRP technique with various percentages of existing steel stirrups (ρ_{sw})

apply NSM reinforcement on top of the existing stirrups to ovoid premature debonding in case remaining cover is small.

6. The comparison between the ultimate load obtained from the FE simulations and the theoretical predictions confirmed the conservative nature of these theoretical formulations in most cases when the shear failure is governed. However, more effort is needed to include the combined effect of internal steel stirrups and NSM CFRP strengthening technique to make these formulations more general.

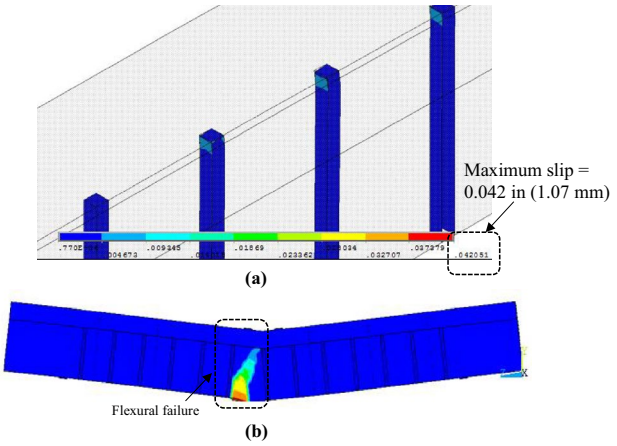

Fig. 10 Failure modes of beam having **a** 0.11% and **b** 0.43% percentage of the internal shear stirrups

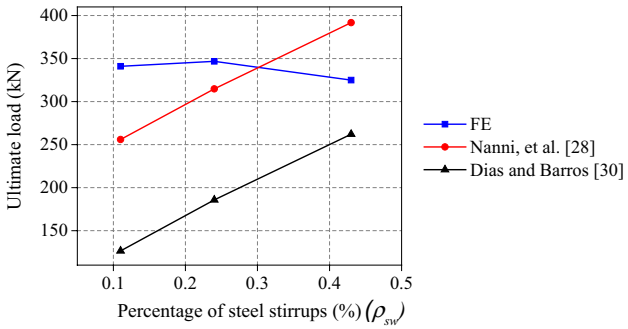

Fig. 11 Comparison of ultimate load of NSM strengthened RC beams obtained from FE simulation with design approach formulations

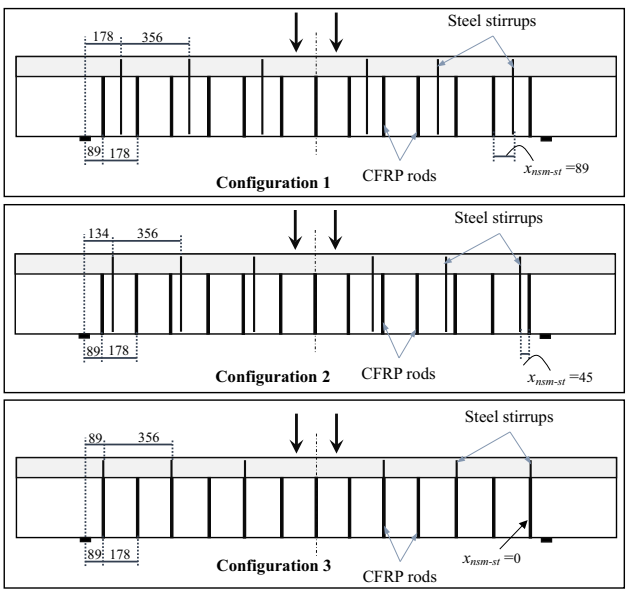

Fig. 12 CFRP configurations

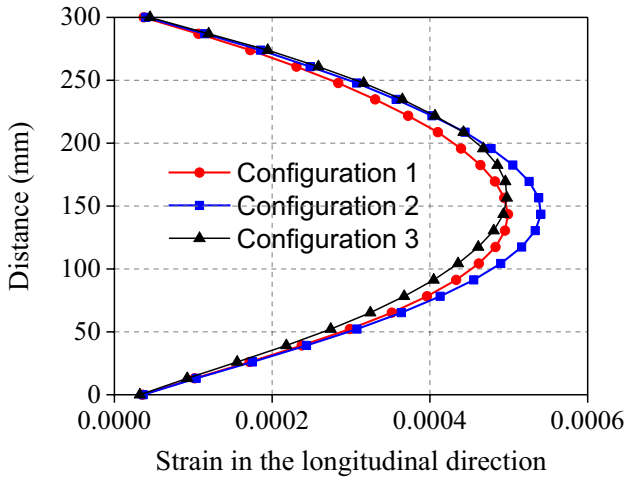

Fig. 13 Strain in the longitudinal direction along the CFRP rod located 534 mm away from the beam centreline

7. Based on the findings of this research, it can be concluded that the NSM strengthening technique can offer a practical and effective solution to protecting the existing RC beams from shear failure.

References

1. Abouzied A, Masmoudi R (2015) Structural performance of new fully and partially concrete-filled rectangular FRP-tube beams. Constr Build Mater 101:652–660
2. Kadhim MMA (2012) Effect of CFRP sheet length on the behavior of HSC continuous Beam. J Thermoplast Compos 25(1):33–44
3. Al-Mahmoud F, Castel A, Minh TQ, François R (2015) Reinforced concrete beams strengthened with NSM CFRP rods in shear. Adv Struct Eng 18(10):1563–1574
4. Jawdhari A, Harik I (2016) Evaluation of RC beams strengthened with spliced CFRP rod panels. In: Proceedings of structural faults and repair
5. Jawdhari A, Peiris A, Harik I (2016) Bond study on CFRP rod panels externally adhered to concrete. J Compos Constr 21(4):04016114
6. Kadhim MMA, Mohammed MJ, Abid AJ (2012) Effect of prestressed CFRP plate location on behavior of RC beam strengthened with prestressed CFRP plate. J Babylon Univ 20(1):105–113
7. Teng J, Lam L, Chen J (2004) Shear strengthening of RC beams with FRP composites. Prog Struct Eng Mater 6(3):173–184
8. Jalali M, Sharbatdar MK, Chen J-F, Alaee FJ (2012) Shear strengthening of RC beams using innovative manually made NSM FRP bars. Constr Build Mater 36:990–1000
9. Al-Sulaimani GJ, Sharif A, Basunbul IA, Baluch MH, Ghaleb BN (1994) Shear repair for reinforced concrete by fiberglass plate bonding. ACI Struct J 91(4):458–464
10. Lee K, Al-Mahaidi R (2003) Strength and failure mechanism of RC T-beams strengthened with CFRP plates. In: Proceedings of the 6th international symposium on FRP reinforcement for concrete structures, Singapore, pp 247–256
11. Khalifa A, Nanni A (2000) Improving shear capacity of existing RC T-section beams using CFRP composites. Cement Concrete Compos 22(3):165–174
12. Adhikary BB, Mutsuyoshi H (2004) Behavior of concrete beams strengthened in shear with carbon-fiber sheets. J Compos Constr 8(3):258–264
13. ACI-440-Committee (2008) Guide for the design and construction of externally bonded FRP systems for strengthening concrete structures. ACI-4402 R-08. American Concrete Institute, Farmington Hills
14. El-Hacha R, Rizkalla SH (2004) Near-surface-mounted fiber-reinforced polymer reinforcements for flexural strengthening of concrete structures. ACI Struct J 101(5):717–726
15. Al-Mahmoud F, Castel A, François R, Tourneur C (2010) RC beams strengthened with NSM CFRP rods and modeling of peeling-off failure. Compos Struct 92(8):1920–1930
16. Nanni A, Ludovico MD, Parretti R (2004) Shear strengthening of a PC bridge girder with NSM CFRP rectangular bars. Adv Struct Eng 7(4):297–309
17. De Lorenzis L, Nanni A (2001) Shear strengthening of reinforced concrete beams with near-surface mounted fiber-reinforced polymer rods. ACI Struct J 98(1):60–68
18. Dias SJ, Barros JA (2013) Shear strengthening of RC beams with NSM CFRP laminates: experimental research and analytical formulation. Compos Struct 99:477–490
19. Dias SJ, Barros JA (2017) NSM shear strengthening technique with CFRP laminates applied in high T cross section RC beams. Compos Part B Eng 114:256–267
20. Dias S, Barros J (2012) NSM shear strengthening technique with CFRP laminates applied in high-strength concrete beams with or without pre-cracking. Compos Part B Eng 43(2):290–301
21. Dias SJ, Barros JA (2012) Experimental behaviour of RC beams shear strengthened with NSM CFRP laminates. Strain 48(1):88–100
22. Dias S, Barros J (2011) Shear strengthening of RC T-section beams with low strength concrete using NSM CFRP laminates. Cement Concrete Compos 33(2):334–345
23. Dias SJ, Barros JA (2010) Performance of reinforced concrete T beams strengthened in shear with NSM CFRP laminates. Eng Struct 32(2):373–384
24. Dias SJ, Barros JA (2008) Shear strengthening of T cross section reinforced concrete beams by near-surface mounted technique. J Compos Constr 12(3):300–311
25. Sabol P, Priganc S (2013) Shear strengthening of concrete members using NSM method. Procedia Eng 65:364–369
26. Sakar G, Hawileh R, Naser M, Abdalla J, Tanarslan M (2014) Nonlinear behavior of shear deficient RC beams strengthened with near surface mounted glass fiber reinforcement under cyclic loading. Mater Design 61:16–25
27. Barros JA, Baghi H, Dias SJ, Ventura-Gouveia A (2013) A FEM-based model to predict the behaviour of RC beams shear strengthened according to the NSM technique. Eng Struct 56:1192–1206
28. Jalali M, Alaee F, Sharbatdar M Numerical investigation on shear strengthening of RC beams using near surface mounted (NSM) FRP. 6th National Congress on Civil Engineering, April 26–27, 2011, Semnan University, Semnan
29. ANSYS (2016) Release 17.2 documentation for ANSYS, Canonsburg
30. Kent DC, Park R (1971) Flexural members with confined concrete. J Struct Div 97:1969–1990
31. ACI-318-14 (2014) Building code requirements for reinforced concrete
32. Chansawat K, Yim SC, Miller TH (2006) Nonlinear finite element analysis of a FRP-strengthened reinforced concrete bridge. J Bridge Eng 11(1):21–32

33. Kachlakev DI, Miller TH, Potisuk T, Yim SC, Chansawat K (2001) Finite element modeling of reinforced concrete structures strengthened with FRP laminates. Dept. of Transportation. Research Group, Oregon
34. Wolanski AJ (2004) Flexural behavior of reinforced and prestressed concrete beams using finite element analysis
35. Omran HY, El-Hacha R (2012) Nonlinear 3D finite element modeling of RC beams strengthened with prestressed NSM-CFRP strips. Constr Build Mater 31:74–85
36. Seracino R, Raizal Saifulnaz M, Oehlers D (2007) Generic debonding resistance of EB and NSM plate-to-concrete joints. J Compos Constr 11(1):62–70
37. Kishi N, Zhang G, Mikami H (2005) Numerical cracking and debonding analysis of RC beams reinforced with FRP sheet. J Compos Constr 9(6):507–514
38. CEB-FIP (1993) Model code 1990. Thomas Telford Services Ltd., London
39. Mofidi A, Chaallal O, Cheng L, Shao Y (2015) Investigation of near surface-mounted method for shear rehabilitation of reinforced concrete beams using fiber reinforced-polymer composites. J Compos Constr 20(2):04015048